Revista Brasileira de Cartografia (2013) N⁰ 65/4: 731-745
Sociedade Brasileira de Cartografia, Geodésia, Fotogrametria e Sensoriamento Remoto
ISSN: 1808-0936

QUANTITATIVE EVALUATION AND QUALITY CONTROL OF COMMERCIALLY ADOPTED TRADITIONAL AND MODERN LIDAR SYSTEM CALIBRATION TECHNIQUES

Avaliação Quantitativa e Controle de Qualidade de Técnicas Tradicionais e Modernas de Calibração de Sistemas LIDAR Empregados Comercialmente

Ana Paula Kersting[1]; Ayman Habib[2] & Mauricio Müller[1]

[1]Instituto de Tecnologia para o Desenvolvimento – LACTEC
Centro Politécnico – Jardim das Américas – Caixa Postal 19067, CEP: 81531-980 – Curitiba – Paraná – Brasil
ana.kersting@lactec.org.br
muller@lactec.org.br

[2]University of Calgary
Department of Geomatics Engineering
2500 University Drive NW, T2N 1N4 – Calgary – Alberta – Canada
ahabib@ucalgary.ca

Recebido em 15 de novembro, 2012/ Aceito em 23 de janeiro, 2013
Received on November 15, 2012/ Accepted on January 23, 2013

ABSTRACT

LiDAR systems have been widely adopted for the collection of topographic data. By integrating the information gathered by navigation sensors (GPS/INS) and a laser ranging/scanning unit, LiDAR systems can directly provide the 3D coordinates of a surface at a high density. In the past decade, LiDAR technology has undergone significant improvements in performance (e.g., higher pulse repetition frequencies, higher operational altitudes) and data processing/post-processing methodologies. Major advances in the data processing include more robust methodologies for the system calibration. Implemented traditional calibration by the service providers are based on iterative sequential estimation of the system parameters that require manual adjustment and time-intensive interaction of a trained operator. In the past few years, automated and more accurate methodologies have become commercially available and have been currently in use by some data providers. In this paper, traditional and modern LiDAR system calibration procedures are evaluated and compared. For that purpose, a practical quality control procedure is used. The underlying concept of the quality control procedure is that in the absence of biases in the system parameters (i.e., for a properly calibrated system), conjugate surface elements in overlapping strips should coincide with each other as well as possible. Incompatibilities between conjugate surface elements in overlapping strips can be used to evaluate the quality of the calibration process. In addition, the presented quality control procedure can be used for diagnosing the cause of detected incompatibilities. More specifically, the detected incompatibilities can be used for estimating the remaining biases in the system parameters. Another advantage of the introduced quality control procedure is the possibility of its implementation by the end user since it only requires the LiDAR point cloud coordinates as well as a general knowledge of the flight configuration. Experimental results have demonstrated significant improvements in the quality of fit among overlapping LiDAR strips when using modern LiDAR system calibration procedures and the ability of the proposed quality control approach to

detect and eliminate remaining biases in the system parameters.

Keywords: Calibration, LiDAR, Accuracy, Error Analysis, Overlapping Strips, Comparative Analysis

RESUMO

Os sistemas LiDAR tem sido vastamente utilizados para a aquisição de dados topográficos. Através da integração das informações obtidas por sensores de navegação (GPS/INS) e por uma unidade laser, os sistemas LiDAR podem obter as coordenadas tridimensionais de uma grande densidade de pontos na superfície do terreno de forma direta. Na última década, a tecnologia LiDAR tem avançado significativamente não somente em termos de desempenho (p.ex.: maiores frequências de repetição, maiores alturas operacionais) como em metodologias de processamento e pós-processamento. Os avanços mais notórios no processamento dos dados abrangem o desenvolvimento de metodologias mais robustas para a calibração do sistema. As metodologias tradicionais de calibração empregadas pelas empresas provedoras de dados consistem de procedimentos iterativos e sequenciais de estimação dos parâmetros, geralmente baseados em ajustamentos manuais e interação exaustiva de um operador experiente. Nos últimos anos, metodologias automatizadas e mais eficientes tem se tornado disponível comercialmente e encontram-se atualmente em uso por algumas empresas provedoras de dados. Neste artigo, procedimentos tradicionais e modernos para calibração do sistema LiDAR são avaliados e comparados. Para este propósito, um método prático de controle de qualidade é empregado. O método é baseado no princípio de que na ausência de erros sistemáticos nos parâmetros do sistema (ou seja, para um sistema adequadamente calibrado), elementos conjugados em faixas sobrepostas do LIDAR devem coincidir o melhor possível. Discrepâncias entre elementos conjugados em faixas sobrepostas podem ser utilizados para avaliar a qualidade do processo de calibração. Além disso, o procedimento de controle de qualidade pode ser utilizado para diagnosticar a causa para as discrepâncias detectadas. Mais especificamente, as incompatibilidades detectadas podem ser usadas para estimar os erros sistemáticos residuais nos parâmetros do sistema. Outra vantagem do procedimento de controle de qualidade apresentado é a possibilidade de sua utilização pelo usuário final uma vez que apenas as coordenadas tridimensionais da nuvem de pontos e conhecimento geral da configuração de voo são requeridos. Os resultados experimentais demonstraram que melhora significativa na qualidade de ajuste entre faixas sobrepostas é obtida quando da utilização de métodos modernos de calibração de sistemas LiDAR. Também foi demonstrada a habilidade do método

1. Introduction

Over the last decade, LiDAR technology has experienced significant improvements in performance (e.g., higher pulse repetition frequencies and operational altitudes) and in data processing/post-processing methodologies. Advances in the data processing (i.e., derivation of X, Y, Z coordinates of the LiDAR point cloud) include better methodologies for the GPS/INS integration as well as higher level of automation in the system calibration procedure. Advances in the data post-processing include the development of automated algorithms for the classification, segmentation, and interpretation of the LiDAR point cloud.

A LiDAR system consists of a laser ranging and scanning unit as well as a position and orientation system (POS), which consists of an integrated differential global positioning system (DGPS) and an inertial navigation system (INS) (Wehr and Lohr, 1999). The ranging unit determines the distance between the laser firing point and its footprint on the ground while the scanning unit allows for a strip-wise data collection. The integrated GPS/INS unit provides the position and attitude information of the platform. The coordinates of the LiDAR points are the result of combining the derived measurements from each of its system components, as well as the system parameters. The relationship between the LiDAR point coordinates, the system parameters, and measurements is expressed through the LiDAR point positioning equation. Such mathematical relationship, which is presented in Equation 1, can be derived through the summation of the vectors ($r_b^m(t)$, r_{lu}^b, and $r_l^{lb}(t)$) as illustrated in Figure 1, after applying the appropriate rotation matrices ($R_b^m(t)$, R_{lu}^b, and $R_{lb}^{lu}(t)$).

where:

$$r_l^m = r_b^m(t) + R_b^m(t) r_{lu}^b + R_b^m(t) R_{lu}^b R_{lb}^{lu}(t) r_l^{lb}(t) \quad (1)$$

$r_b^m(t)$: is the vector from the origin of the ground reference frame to the origin of the IMU coordinate system derived through the GPS/INS integration process while considering the lever arm between the IMU body frame and the phase center of the GPS antenna;

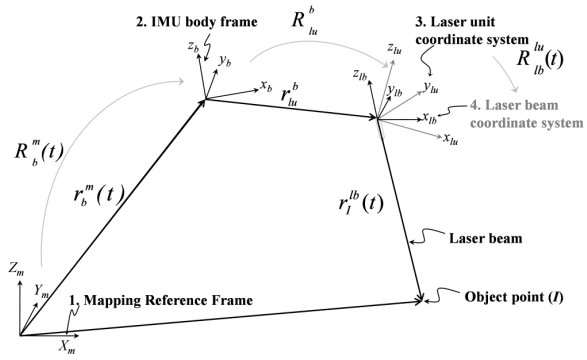

Fig. 1 - Coordinate systems and involved quantities in the LiDAR point positioning equation.

– η_{lu}^{b}: is the lever arm defined by $(\Delta X, \Delta Y, \Delta Z)$, which is the vector from the origin of the IMU coordinate system to the origin of the laser unit coordinate system (defined relative to the IMU body frame);

– $r_l^{lb}(t) = \begin{bmatrix} 0 \\ 0 \\ -(\rho + \Delta\rho) \end{bmatrix}$: is the laser range vector whose magnitude (ρ) is equivalent to the distance from the laser firing point to its footprint and $\Delta\rho$ is a constant bias in the laser range vector;

– $R_b^m(t)$: is the rotation matrix relating the ground and IMU coordinate systems, which is derived through the GPS/INS integration process;

– R_{lu}^{b}: is the rotation matrix relating the IMU and laser unit coordinate systems, which is defined by the boresight pitch, roll, and yaw angles $(\Delta\omega, \Delta\varphi, \Delta\kappa)$ – assuming the Y-axis of the IMU body frame to be aligned along the flying direction;

– $R_{lb}^{lu}(t) = \begin{bmatrix} cos\, S\beta(t) & 0 & sin\, S\beta(t) \\ 0 & 1 & 0 \\ -sin\, S\beta(t) & 0 & cos\, S\beta(t) \end{bmatrix}$: is the rotation matrix relating the laser unit and laser beam coordinate systems, which is defined by the mirror scan angle *â(t)* (considering a linear scanner). The term S is the mirror angle scale.

The involved quantities in the LiDAR equation are all measured during the acquisition process except for the system parameters, i.e., the mounting parameters relating the system components – the boresight pitch, roll, and yaw angles $(\Delta\omega, \Delta\varphi, \Delta\kappa)$ and the lever arm components $(\Delta X, \Delta Y, \Delta Z)$ – as well as systematic errors in the laser unit measurements – the constant bias in the laser range vector $(\Delta\rho)$ and the mirror angle scale (*S*). Such parameters are determined through a calibration process. The LiDAR system calibration process involves several steps such as the calibration of the individual system components in a laboratory, which is usually performed by the system manufacturer, and a platform calibration to determine the system mounting parameters (Schenk, 2001). An in-flight system calibration is finally conducted to refine the determined parameters during the laboratory and platform calibrations. When the LiDAR systems became commercially available in the late 90´s and until very recently, the traditional in-flight calibration procedures used in the industry have several shortcomings such as (i) the use of manual adjustments and empirical procedures, (ii) time consuming and expensive, (iii) the use of complicated and sequential procedures, and (iv) strong dependence on control surfaces. Moreover, until now there is no commonly accepted methodology since the calibration techniques are usually based on a manufacturer software package and the expertise of the LiDAR data provider. As a result of the non-transparent and empirical calibration procedures, systematic discrepancies between conjugate surface elements in overlapping strips have been observed in the collected data, which means that the potential accuracy has not been fully achieved. For this reason, significant research effort has been put towards the development of efficient and robust calibration methodologies by the scientific community in the last decade (Burman, 2000; Filin, 2001; Morin, 2002; Toth, 2002; Friess, 2006; Skaloud and Lichti, 2006; Habib et al., 2010b; Kersting, 2011; Kersting et al., 2012). The developed procedures utilize automated adjustments procedures based on the physical sensor model relating the system measurements/parameters to the ground coordinates of the LiDAR points while either incorporating the system's raw data (e.g., Filin, 2001; Skaloud and Lichti, 2006; Friess, 2006; Kersting, 2011; Kersting et al., 2012) or at least the trajectory and time-tagged point cloud (Burman, 2000; Toth, 2002; Morin, 2002; Habib et al., 2010b) for the estimation of the system parameters with the help of the LiDAR equation. Such calibration

procedures are denoted as rigorous calibration procedures when the system raw measurements are used or quasi-rigorous when only the trajectory and the time-tagged LiDAR point cloud are utilized. Existing approaches differ in terms of the estimated system parameters, used primitives, as well as pre-processing and ground control requirements.

Advances in the scientific community have also become commercially available in the last few years. An example is the available calibration procedure in the Optech's most current data processing software (*LMS – LiDAR Mapping Suite*). The calibration procedure was introduced by Peter Friess (Friess, 2006), who further developed it into a commercially available software tool since 2010. In this paper, a comparative analysis between the available traditional and modern rigorous calibration procedures to the industry is performed. More specifically, the previously employed calibration procedure by LACTEC for the Optech's ALTM2050 system (which is based on manual and iterative adjustment) is compared with the LMS calibration procedure, which is currently in use by LACTEC for the calibration of the ALTM 2050 and the recently purchased Pegasus HD500 system. To evaluate and compare these procedures, a practical and meaningful quality control procedure (Habib et al., 2009) is employed. The paper starts by briefly outlining the used calibration procedures in the industry which will be evaluated/compared in this paper. Then, the utilized quality control procedure for the evaluation of the calibration procedures is described. Experimental results using real datasets acquired by the ALTM 2050 system are performed. Finally, some concluding remarks and recommendations for future work are outlined.

2. LIDAR SYSTEM CALIBRATION

The LiDAR system calibration is usually accomplished in several steps: (i) Laboratory calibration, (ii) Platform calibration, and (iii) In-flight calibration. In the laboratory calibration, which is conducted by the system manufacturer, the individual system components are calibrated. In addition, the lever arm and boresight angles between the laser unit mirror and the IMU as well as the lever arm between the IMU and the sensor reference point are determined (Figure 2). In the platform calibration, the lever arm between the sensor reference point and the GPS antenna is determined (Figure 2). Since the determined parameters in the laboratory and platform calibrations might be biased and/or not stable over time, an in-flight calibration should be continuously performed by the service providers.

The used traditional calibration by the service providers consist of iterative procedures and manual adjustments of the calibration parameters. Such procedures usually demand several flight lines with specific configuration and are highly dependent on control information with specific characteristics (e.g., large building with particular dimensions). The discrepancies between the LiDAR point cloud coordinates and control surfaces are derived through manual procedures or a manufacturer-provided software package. Then, such discrepancies are used to obtain rough estimates for the biases/corrections to the system parameters. The dataset is reprocessed using this new set of system parameters. The entire procedure is repeated until the corrections to the system parameters become smaller than a pre-established threshold. Thus, the

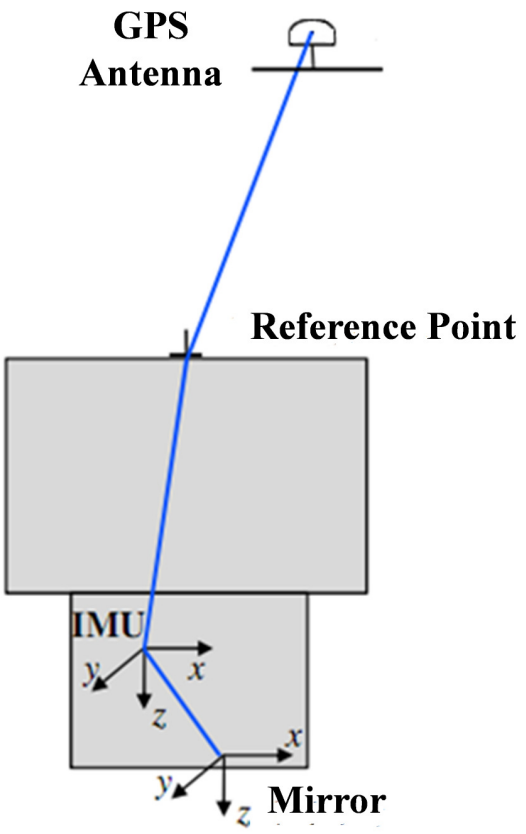

Fig. 2 – Estimated lever arms during the laboratory and platform calibrations.

system parameters are not refined simultaneously; instead, they are refined sequentially, following a particular order. Besides the requirement of a large amount of control information and flight time, significant amount of manual interaction is involved. Table 1 presents the originally recommended control and flight configuration by the system manufacturer (Optech) for the calibration of the ALTM 2050 system, previously adopted by LACTEC. All the flight lines are acquired using one flying height only (1000m). In this calibration procedure, the following parameters are refined: the angular offset (index error), the boresight pitch and roll angles, the mirror angle scale, and the range.

The acquired strips in profile mode are used for the determination of the angular offset (index error) and the boresight pitch angle bias. The angular offset is determined by looking at the raw LiDAR data. The average of the reported deviations from 0º in the scan angles are used as the angular offset corrections. This average is derived from at least three strips. To determine the boresight pitch angle correction, incident pulses on the building edge are compared with the control edge (determined by accurate field survey). More specifically, a boresight pitch angle correction is derived using the discrepancy between the control edge and the incident LiDAR point on the edge and the flying height above the building. The correction is applied and the data is reprocessed. This iterative procedure stops when the improvement is smaller than a pre-established threshold (0.01º). The boresight roll angle correction is determined next using the strips with 5º mirror scan angle. Similar to the boresight pitch angle correction, the boresight roll angle correction is determined by comparing incident pulses on the building edge with the control edge. The incident LiDAR pulses on the building edge (when computing both the boresight pitch and roll angle corrections) are identified whenever the elevation of the first return differs from that for the last return. The mirror angle scale correction and range bias are determined using 4 strips flown perpendicular to the airport runway in scan mode (20º mirror scan angle). The vertical discrepancies between the LiDAR points and the control points at the scan edge are utilized to obtain the mirror angle scale correction. Finally the range error is determined by comparing the height of the LiDAR coordinates to the control data. One should note that the lever arm and the boresight yaw angle are not refined in this calibration procedure. More specifically, the service provider has to rely on the estimated parameters during the laboratory and platform calibrations.

The recently released data processing software by Optech, the *LMS* (*LiDAR Mapping Suite*), which is currently in use by LACTEC, has an automated calibration procedure, which is embedded in the data processing routine. The underlying concept of this calibration procedure is to estimate the system parameters that minimize the discrepancies between conjugate planes, which are extracted from overlapping LiDAR strips (through a segmentation process), in a least squares adjustment procedure

Different from the traditional calibration procedure, there is no user interaction in the process. Moreover, no particular flight scanning mode is required. Since appropriate primitives are used to

Table 1: Flight and control configuration requirements (recommended by the system manufacturer) for the previously adopted procedure by LACTEC for the calibration of the Optech ALTM 2050 system

Control Information	- Boundaries of a building with a minimum height of 5 meters and a length of 70 to 100 meters - Control points over an airport runway
Flight Configuration	- **4 flight lines** in profile mode (0° mirror scan angle) (Figure 3a) and **4 flight lines** with 5° mirror scan angle (Figure 3b) over the building with known boundaries - **4 flight lines** with 20° mirror scan angle over an airport runway

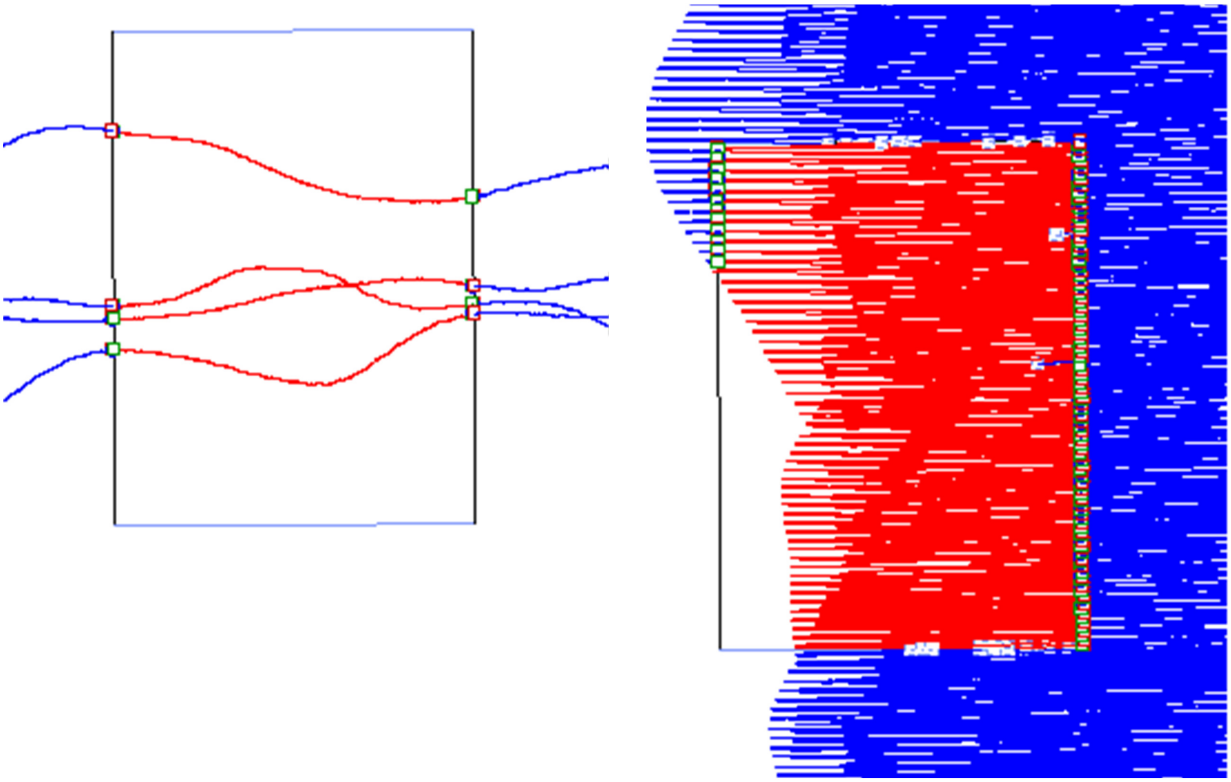

(a)

In red: Incident points on the building rooftop
In blue: Incident points on the ground
Boxes: Incident points on the building edge

(b)

In red: Incident points on the building rooftop
In blue: Incident points on the ground
Boxes: Incident points on the building edge

Fig. 3 – (a) Flight lines in profile mode (b) Flight lines with 5º mirror scan angle (Kersting and Martins, 2006) over a large building with known boundaries.

deal with the LiDAR point cloud (i.e., conjugate planes), the density of the point cloud does not have an impact on the accuracy of the estimated parameters, as long as enough returns for the derivation of conjugate planes are available. Actual project flight lines can be used for the LMS calibration procedure. The system manufacturer recommends the use of flight lines in opposite and cross directions (optionally a diagonal one) from a flying height of 1000m, preferably over an urban area. In the LMS calibration, the following parameters can be refined: all the boresight angles (pitch, roll, and yaw) and the mirror angle scale. Derived parameters from the laboratory/platform calibration (e.g., the lever arm components) are not refined in the LMS calibration process. The range bias is determined using control points over the airport runway (done by the system manufacturer and periodically by the service provider using another software package). Except for the range bias estimation, control information is not required for the in-flight system calibration. Besides the above mentioned calibration system parameters, *LMS* has a "production" mode where the user can solve for flight line specific parameters for a final refinement of the data. In the experimental results section, the traditional and the LMS calibration procedures are evaluated and compared using a practical/reliable quality control procedure, which is described next.

3. QUALITY CONTROL PROCEDURE

As suggested by Habib et al. (2009), the utilized quality control procedure is based on evaluating the degree of consistency among conjugate surface elements in overlapping strips to check the internal/relative quality of the LiDAR data. The conceptual basis of that procedure is that conjugate surface elements in overlapping strips should coincide with each other in the absence of systematic errors. If consistent discrepancies are detected, then one can infer the presence of biases in the system parameters and/or measurements. The quality control process is accomplished in two steps. First, the quality of fit between conjugate surface elements

is evaluated using a discrepancy detection procedure. Then, a diagnostic component is utilized to relate the detected discrepancies to the remaining biases in the system parameters through a derived mathematical model after making some assumptions regarding the flight and ground coverage configuration.

3.1. Discrepancy Detection Procedure

To properly deal with the irregular nature of the LiDAR point cloud, higher order primitives are utilized in the discrepancy detection procedure. The utilized primitives consist of conjugate point-patch pairs. More specifically, one strip is represented by the original points, while the other strip is represented by triangular patches, which can be derived from a Triangular Irregular Network (TIN) generation procedure. In contrast to the primitives used in the LMS software (i.e., conjugate planes), the primitives used in the quality control procedure do not require preprocessing of the LiDAR point cloud to extract planar features (i.e., segmentation process).

As shown in Figure 4, if the point q_i in S_2 belongs to the triangular patch S_p represented by the vertices S_{p_a}, S_{p_b}, and S_{p_c} in S_1, then this point should coincide with that patch in the absence of systematic errors in the system parameters/ measurements. In the presence of systematic errors, there will be a discrepancy between the point and the correspondent patch. The quality control procedure estimates the transformation parameters that minimize such discrepancy. In Habib et al. (2010a), it is demonstrated that the discrepancies between parallel strips in the presence of the biases in the system parameters (biases in the lever arm, boresight angles, mirror angle scale, and range) can be modeled by 3 shifts (X_T, Y_T, Z_T) and a rotation angle around the flight line ($\ddot{O}$). Although the considered systematic errors in this research would lead to three shifts and one rotation around the flight direction, we can consider a general transformation function involving three rotation angles in order to check for the presence of other biases, such as unmodeled biases in the system parameters and/or GPS/INS navigation errors. After applying the appropriate transformation parameters (i.e., the detected discrepancies), the volume of the pyramid whose vertices are $q_i 2$, S_{p_a}, S_{p_b}, and S_{p_c} should be zero. Such a volume constraint can be mathematically described by Equation 2. Using multiple point-patch pairs, we can estimate the transformation parameters which satisfy the volume constraints. The solution to the defined constraints after the linearization shown in Equation 3 can be derived through Equation 4. For reliable estimation of the transformation parameters (discrepancies), the utilized patches should have a balanced distribution of slopes and aspects.

$$\begin{vmatrix} X_{q_i'} & Y_{q_i'} & Z_{q_i'} & 1 \\ X_{p_a} & Y_{p_a} & Z_{p_a} & 1 \\ X_{p_b} & Y_{p_b} & Z_{p_b} & 1 \\ X_{p_c} & Y_{p_c} & Z_{p_c} & 1 \end{vmatrix} = 0 \qquad (2)$$

where,

$$\begin{bmatrix} X_{q_i'} \\ Y_{q_i'} \\ Z_{q_i'} \end{bmatrix} = \begin{bmatrix} X_T \\ Y_T \\ Z_T \end{bmatrix} + R(\Omega, \Phi, \mathrm{K}) \begin{bmatrix} X_{q_i} \\ Y_{q_i} \\ Z_{q_i} \end{bmatrix} \qquad (3)$$

$$w = A\,x + B\,e \qquad e \sim (0, \Sigma_Y)$$

where,

– x are the corrections to the approximate values of the unknown parameters $(X_T, Y_T, Z_T, \Omega, \Phi, \mathrm{K})$,

– A is the partial derivative matrix w.r.t. the unknown parameters,

– B is the partial derivative matrix w.r.t. the points' coordinates,

– w is the estimated determinant using the approximate values for the unknown parameters and points' coordinates, and

– Σ_Y is the apriori variance-covariance matrix of the points' coordinates.

The correspondences between points in S_2 and patches in S_1 are established through an automated matching strategy. More specifically, the correspondence is performed in an iterated manner, using the Iterative Closest Patch (ICPatch) procedure. For more details refer to Habib et al. (2009) and Habib et al. (2010a).

$$\hat{x} = [A^T (B\,\Sigma_Y\,B^T)^{-1}\,A]^{-1}\,A^T (B\,\Sigma_Y\,B^T)^{-1}\,w$$
$$B\,\tilde{e} = w - A\,\hat{x}$$
aposteriori variance factor :
$$\hat{\sigma}_o^2 = \tilde{e}^T B^T\,(B\,\Sigma_Y\,B^T)^{-1}\,B\,\tilde{e} / redundancy \qquad (4)$$
aposteriori variance - covariance matrix :
$$\tilde{\Sigma}_Y = \hat{\sigma}_o^2\,\Sigma_Y$$

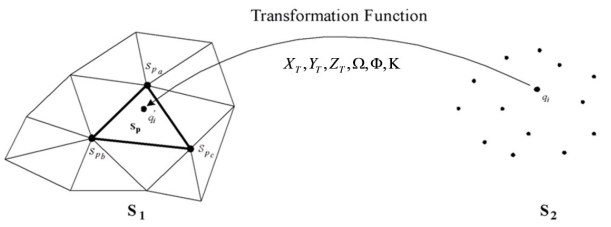

Fig. 4 – Conceptual basis of the proposed point-to-patch correspondence procedure (Adapted from Habib et al., 2010a).

3.2. Diagnostic Component

To diagnose the cause of the detected incompatibilities among conjugate surface elements in overlapping strips, the estimated discrepancies (transformation parameters) are related to the remaining biases in the system parameters. The derivation of the utilized mathematical relationship is detailed in Habib et al. (2009). The following assumptions are considered to derive the relationship between the system biases and the discrepancies between overlapping strip pairs: (i) linear scanner, (ii) straight-line trajectories with flying directions parallel to the positive and negative directions of the Y-axis of the ground coordinate system, (iii) vertical system (small pitch and roll angles), (iv) small boresight angles, (v) terrain and surface height variation is small relative to the flying height, and (vi) the utilized convention for the laser scanner and IMU body frame coordinate systems is right-forward-up (i.e., right-handed coordinate system).

The mathematical model expressing the relationship between the remaining biases in the system parameters and the discrepancies between overlapping strip pairs, which are flown in opposite directions, is presented in Equation 5. For overlapping strip pairs flown in the same direction, the mathematical relationship is shown in Equation 6. The multiple signs ($\mp,\pm$) in Equations 5 and 6 depend on the relationship between the forward and backward strips; with the top sign used when the forward strip is to the right of the backward strip. The forward strip corresponds to the flight line flown along the positive direction of the Y-axis of the ground coordinate system. The discrepancies should be estimated using the forward strip as the reference one. One should note in Equations 5 and 6 that only the bias in the vertical lever arm component cannot be detected using overlapping strip pairs. The reason is that the impact of such bias is the same for all the strips regardless of the utilized flight configuration.

Although biases in the range vector causes discrepancies among strips with some overlap percentage, such discrepancies are quite small. To reliably solve for the range bias, control information should be used. Examining Equations 5 and 6, one can determine the flight configuration that maximizes the impact of systematic errors and establish the optimal flight configuration, which decouples various systematic errors. For example, closer inspection of Equation 6 reveals that parallel strips with the least amount of necessary overlap (i.e., the largest possible lateral distance D) for identifying conjugate surface elements are useful for magnifying the impact of biases in the boresight yaw and roll angles, mirror angle scale, and range. Equation 5 reveals that the boresight pitch angle can be decoupled from the lever arm component in the along-flight direction by having strip pairs from two different flying heights. Working with two strip pairs which are captured from two flying heights in opposite directions with 100% overlap (i.e., D=0) are optimal for the recovery of the biases in the planimetric lever arm components as well as the boresight pitch and roll angles (Equation 7). Therefore, the optimum flight configuration for reliable estimation of the remaining biases in the system parameters through the diagnostic component of the quality control procedure should include four flight lines that are flown in opposite directions with 100% overlap from two different flying heights as well as parallel flight lines with the least amount of overlap possible (Kersting, 2011).

where:

– D : is the lateral distance between the two flight lines in question;

– H : flying height above ground;

– $\delta\Delta X$: is the bias in the lever arm component in the across-flight direction;

– $\delta\Delta Y$: is the bias in the lever arm component in the along-flight direction;

$$\begin{bmatrix} X_T \\ Y_T \\ \Phi \end{bmatrix} = \begin{bmatrix} 2\delta\Delta X - 2H\delta\Delta\varphi \mp D/H\ \delta\Delta\rho \mp D\delta S \\ 2\delta\Delta Y + 2H\delta\Delta\omega \mp D\delta\Delta\kappa \\ 2\delta\Delta\varphi \pm 2\dfrac{D}{H}\delta S \end{bmatrix} \quad (5)$$

$$\begin{bmatrix} X_T \\ Y_T \\ Z_T \\ \Phi \end{bmatrix} = \begin{bmatrix} \mp D/H\ \delta\Delta\rho \mp D\delta S \\ \mp D\delta\Delta\kappa \\ \pm D\delta\Delta\varphi \\ \pm 2\dfrac{D}{H}\delta S \end{bmatrix} \quad (6)$$

– $\delta\Delta\omega$: is the bias in the boresight pitch angle;
– $\delta\Delta\varphi$: is the bias in the boresight roll angle;
– $\delta\Delta\kappa$: is the bias in the boresight yaw angle;
– δS : is the bias in the mirror angle scale.

$$\begin{bmatrix} X_T \\ Y_T \\ \Phi \end{bmatrix} = \begin{bmatrix} 2\delta\Delta X - 2H\delta\Delta\varphi \\ 2\delta\Delta Y + 2H\delta\Delta\omega \\ 2\delta\Delta\varphi \end{bmatrix} \quad (7)$$

The main advantage of the diagnostic component of the quality control procedure is that the remaining biases in the system parameters can be estimated without the need for raw measurements. By just having the knowledge of the general parameters of the flight configuration, the end user can utilize the quality control procedure to diagnose the system (i.e., identify the origin of detected discrepancies) and improve the quality of the point cloud coordinates by removing the impact of the remaining biases in the system parameters.

4. EXPERIMENTAL RESULTS

To evaluate the performance of the different calibration techniques, a dataset captured by the Optech ALTM 2050 system was utilized. The dataset is also used to evaluate the ability of the quality control procedure to detect the discrepancies among overlapping strips following the adjustment of the point cloud coordinates using the estimated parameters from the different calibration techniques. Moreover, we aim at using this dataset to confirm the ability of the diagnostic component of the quality control procedure to correctly identify the remaining biases in the system parameters after the calibration and point cloud adjustment. The dataset includes both flight lines over an urban area and an airport runway. The flight mission is designed to provide the necessary data for the traditional calibration (as indicated in Table 1), the LMS calibration, and the diagnostic component of the quality control procedure. The flight lines over the urban area are illustrated in Figure 5. In addition to these flight lines, four flight lines were acquired over an airport runway where ground control points were available. The traditional calibration technique utilizes the flight lines over the runway to estimate the range bias and mirror angle scale. Table 2 lists the characteristics of all the flight lines over the urban area and the airport runway.

The traditional calibration procedure was performed using flight lines 1 to 8 and 15 to 18. As can be seen in Table 2, these strips are acquired from a flying height of 1000m. As mentioned earlier, the traditional calibration procedure sequentially estimates the biases in the system parameters according to the following order: angular offset, boresight pitch angle, boresight roll angle, mirror angle scale, and range. Flight lines 1 to 4, which were acquired in profile mode (0º mirror scan angle) over a large building with known boundaries, were used to estimate the biases in the angular offset and the boresight pitch angle. Flight lines 5 to 8, which were acquired using a 5º mirror scan angle over a large building with known/surveyed boundaries, were used to estimate the bias in the boresight roll angle. The flight lines over the runway (15 to 18) were used to estimate the bias in the mirror angle scale and range. In the LMS calibration, flight lines 5 to 14, which correspond to the flight lines in Figure 5 after excluding the flight lines acquired in profile mode, were used.

To evaluate the traditional and LMS calibration techniques, the quality control procedure

Table 2: Characteristics of the acquired flight lines by the Optech ALTM 2050 system

Flight line	Flying Height (m)	Scan Angle (º)	Covered Area
1	1000	0	
2	1000	0	
3	1000	0	
4	1000	0	
5	1000	5	
6	1000	5	
7	1000	5	Urban area
8	1000	5	
9	1000	20	
10	1000	20	
11	2000	20	
12	2000	20	
13	2000	20	
14	2000	20	
15	1000	20	
16	1000	20	Airport Runway
17	1000	20	
18	1000	20	

presented in section 3 was employed. The used strip pairs for the discrepancy detection are listed in Table 3.

The quality control procedure is performed in two steps. First, discrepancies between the overlapping strip pairs, which are reconstructed after adjusting the point cloud coordinates using the estimated system parameters from the different calibration procedures, are derived. Then, the diagnostic component is performed to identify the remaining biases in the system parameters using the detected discrepancies (Equations 5 and 6).

Tables 4 and 5 report the detected discrepancies between the reconstructed strip pairs after adjusting the point cloud coordinates using the estimated system parameters from the traditional and the LMS calibration techniques, respectively. The detected discrepancies (X_T, Y_T, Z_T, Ù, Ö, Ê) were recalculated to produce a new set of parameters (X_T', Y_T', Z_T', Ù', Ö', Ê') that correspond to a coordinate system where the flight direction is parallel to the Y-Axis. This recalculation is necessary to comply with the requirements of the diagnostic component of the quality control procedure. Table 4 reports large discrepancies among the strip pairs 11&12 and 13&14, which are captured from a 2000m flying height, in the along-flight direction (Y-axis). The strip pairs 5&6 and 5&7, which are captured from a 1000m flying height, have discrepancies of lower magnitude. As mentioned earlier, the traditional calibration procedure is performed using flight lines acquired from 1000m flying height. The larger magnitude of detected discrepancies among the captured strip pairs from a 2000m flying height indicates a problem in some of the boresight angles. The impact of inaccuracies in boresight angles is amplified by an increase in the flying height. As can be seen in Table 5, the LMS calibration is producing strips with higher level of compatibility (i.e., lower discrepancies are detected when compared to Table 4). Although of smaller magnitude, the detected discrepancies in Table 5 are still large for an automated calibration procedure that simultaneously estimates the system parameters. This level of discrepancies is an indication that either some of the system parameters are not modeled or there is a problem with the estimated parameters. Although the system manufacturer recommends the system calibration using strips from a single flying height, the utilized strips for the LMS calibration are captured from 1000m and 2000m flying heights. To investigate the cause of the incompatibility associated with the LMS procedure, we performed the calibration and quality control using strip pairs captured from a single flying height at a time. Table 6 reports the detected discrepancies among strip pairs that are captured from the same flying height as the used strips in the calibration procedure. The reported discrepancies in Table 6 are much smaller than those in Table 5. As a further investigation, we report the detected discrepancies among the adjusted strip pairs from 2000m flying height using the estimated parameters from the LMS calibration on the captured strips from the 1000m flying height (Table 7). It is quite obvious that the detected discrepancies in Table 7 are even worse than those in Tables 5. Therefore, one can hypothesize that the reported numbers in Tables 5, 6, and 7 indicate the presence of remaining biases in some of the boresight angles.

Table 3: Characteristics of the utilized overlapping LiDAR strip pairs for the quality control procedure

Strip pairs	Flying Direction	% Overlap	Average Lateral Distance *D* (m)	Average Flying Height *H* (m)
11&12	Opposite	100	0	2000
13&14	Opposite	90	75	2000
5&6	Opposite	100	0	1000
5&7	Parallel	75	20	1000

To get an additional insight of the origin of the detected discrepancies in Tables 4 and 5, the diagnostic component of the quality control procedure was used to relate these discrepancies to the remaining biases in the system parameters using Equations 5 and 6. The estimated remaining biases for the traditional and the LMS calibration procedures are reported in Table 8. As can be seen in this table, the largest remaining bias after the traditional calibration is in the boresight yaw angle followed by biases in the boresight pitch angle and the lever arm components in the along-flight direction – of larger magnitude – and the across-flight direction – of smaller magnitude. In this regard, one should note that neither the boresight yaw angle nor the lever arm is estimated within the traditional calibration. As it has been mentioned in the analysis of Equations 5 and 6, the lever arm component in the along-flight direction would be correlated with the boresight pitch angle for captured flight lines from

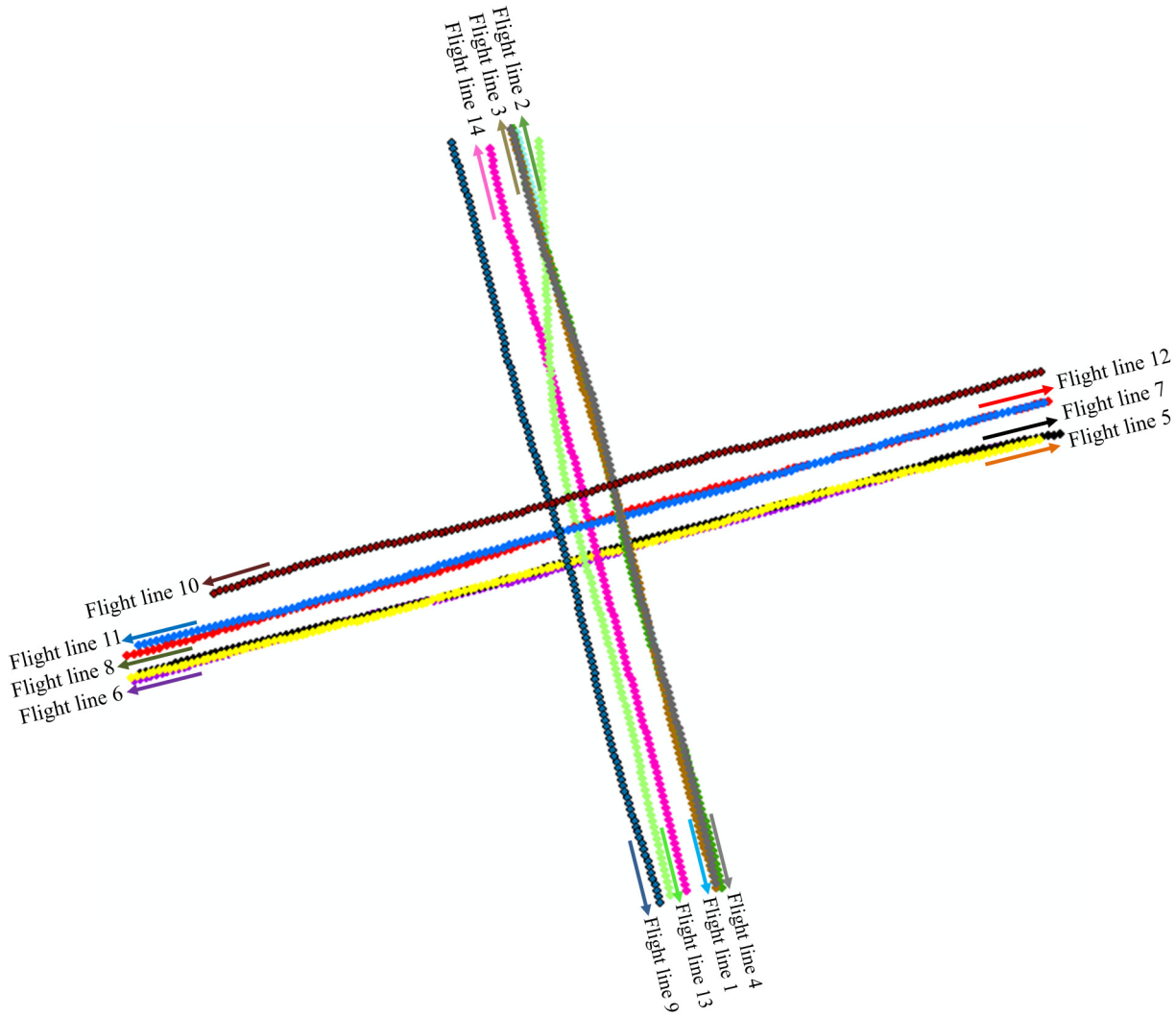

Fig. 5 – Flight lines acquired by the Optech ALTM 2050 system over an urban area.

a single flying height. Since the traditional calibration is based on flight lines from a single flying height, the estimated boresight pitch angle is erroneously estimated to compensate for the lever arm component in the along-flight direction, which is not considered in the traditional calibration. This erroneous estimation of the boresight pitch angle will only be visible when dealing with flight lines from a different flying height since the impact of the boresight pitch is flying height dependent while the impact of the lever arm component is flying height independent. This is quite evident in Table 4 where one can see that the reported discrepancies for the captured strips from 2000m flying height are larger than those detected for the captured strips from the 1000m flying height. Although, a bias in the boresight yaw angle would cause a discrepancy among the strip pairs in the along-flight direction which could impact the validity of the estimated boresight pitch angle, one can still declare that this would not be the case for the traditional calibration. The independence of the estimated bias in the boresight pitch angle from the un-modeled bias in the boresight yaw angle is due to the fact that captured flight lines in profile mode (i.e., 0º mirror scan angle) are used for the estimation of the bias in the boresight pitch angle. For this type of flight lines, a bias in the boresight yaw angle would not have any effect on the derived point cloud coordinates (the impact of the boresight yaw angle is linearly dependent on the scan angle). Therefore, the reported discrepancies in Table 4 can be attributed to remaining biases in the boresight pitch and yaw angle as well as the lever arm components in the along-flight and across-flight direction.

Looking at the estimated remaining biases after the LMS calibration by the diagnostic component of the quality control procedure, one can also see the same magnitude of biases in the lever arm components in the along-flight and across-flight

directions as those reported for the traditional calibration. This should be expected since both procedures do not consider any biases in the lever arm components. The other significant bias for the LMS calibration is the one observed in the boresight pitch angle. Since the LMS calibration is conducted using captured flight lines from 1000m and 2000m flying heights, one can conclude the boresight pitch angle and the lever arm component in the along-flight direction are decoupled. However, the LMS calibration aims at minimizing the discrepancies between conjugate features in the along-flight direction, which are caused by both the boresight pitch angle and the lever arm component in the along-flight direction, by only modifying the boresight pitch angle. Therefore, the bias in the boresight pitch angle was estimated to achieve the best proximity in the along-flight direction between derived planar features from different flying heights. The varying flying heights led to a smaller impact of the un-modeled bias in the lever arm component in the along-flight direction on the boresight pitch angle (this is why the remaining bias in the boresight pitch angle for the LMS calibration is of smaller magnitude when compared to the one in the traditional calibration – refer to Table 8). In other words, dealing with two flying heights in the LMS calibration had a positive impact on coming up with a better estimate of the boresight pitch angle when compared with the traditional calibration. Therefore, even if the manufacturer recommends the utilization of flight lines from a single flying height for the LMS calibration, one should use different flying heights to come up with a better estimate of the boresight pitch angle in case there are still biases in the lever arm component in the along-flight direction.

Table 9 reports the detected discrepancies between the reconstructed strip pairs after adjusting the point cloud to remove the remaining biases as derived by the diagnostic component of the quality control procedure. Once again, the reported discrepancies in Table 9 were recalculated to correspond to a coordinate system where the flight direction is parallel to the Y-Axis. One can note that the overlapping strip pairs become quite compatible, which demonstrates the validity of the quality control procedure to reliably diagnose and identify the origin of the detected discrepancies. Therefore, the proposed quality control procedure can be thought of as a calibration procedure that derives the remaining biases in the system parameters after a given calibration. Finally, the LMS calibration was redone while using the refined lever arm components in the along-flight and across-flight directions by the quality control procedure (i.e., ÄX = -0.06m and ÄY = -0.19m). Table 10 reports the estimated discrepancies between the reconstructed strip pairs using the system parameters from the second LMS calibration. We can observe in Table 10 that the strip pairs became quite compatible, which demonstrates comparable results with the ones obtained in Table 9. Therefore, the LMS calibration can be considered to be an accurate calibration procedure as long as the lever arm components are reliable.

4. Conclusions and Recommendations for Future Research

This paper provides a comparative analysis of the traditional and newly available LiDAR calibration procedures that are adopted by the industry. To compare and evaluate such techniques, a quality control procedure has been introduced. The underlying conceptual basis of the quality control procedure is that for a properly calibrated system and in the absence of navigation errors, there should be no discrepancies between overlapping strip pairs. Significant discrepancies are indications of biases in the system parameters and/or measurements or the presence of un-modeled systematic errors. Besides detecting discrepancies between the overlapping strip pairs, the quality control procedure has a diagnostic component that allows for the identification of the remaining biases in the system parameters after the different calibration techniques. The estimation of the remaining biases in the system parameters through the diagnostic component of the quality control procedure requires having four flight lines that are flown in opposite directions with 100% overlap from two different flying heights as well as parallel flight lines with the least amount of overlap possible.

The main characteristics of traditional and modern calibration procedures presented in this paper can be summarized as follows:

- User interaction:
- Traditional Calibration: Involves manual/empirical a justments
- LMS Calibration: No user interaction
- Control requirement:

Table 4: Detected discrepancies (I.E., three shifts and three rotations) between the reconstructed strip pairs using the estimated system parameters from the traditional calibration procedure

11&12 (2000m)			13&14 (2000m)			5&6 (1000m)			5&7 (1000m)		
X_T' (m)	Y_T' (m)	Z_T' (m)	X_T' (m)	Y_T' (m)	Z_T' (m)	X_T' (m)	Y_T' (m)	Z_T' (m)	X_T' (m)	Y_T' (m)	Z_T' (m)
-0.08	0.77	-0.01	0.01	0.74	0.01	0.08	0.21	-0.02	-0.06	-0.09	0.00
Ω' (°)	Φ' (°)	K' (°)	Ω' (°)	Φ' (°)	K' (°)	Ω' (°)	Φ' (°)	K' (°)	Ω' (°)	Φ' (°)	K' (°)
0.00082	-0.00157	-0.00100	-0.00009	-0.00691	0.00360	-0.00061	-0.00615	-0.00200	0.00002	-0.00730	-0.00170

Table 5: Detected discrepancies (I.E., three shifts and three rotations) between the reconstructed strip pairs using the estimated system parameters from the LMS calibration procedure

11&12 (2000m)			13&14 (2000m)			5&6 (1000m)			5&7 (1000m)		
X_T' (m)	Y_T' (m)	Z_T' (m)	X_T' (m)	Y_T' (m)	Z_T' (m)	X_T' (m)	Y_T' (m)	Z_T' (m)	X_T' (m)	Y_T' (m)	Z_T' (m)
-0.20	0.28	-0.01	-0.12	0.33	0.04	0.16	-0.04	-0.03	-0.08	-0.08	0.02
Ω' (°)	Φ' (°)	K' (°)	Ω' (°)	Φ' (°)	K' (°)	Ω' (°)	Φ' (°)	K' (°)	Ω' (°)	Φ' (°)	K' (°)
0.0006	0.0099	-0.0012	0.0007	0.0038	0.0026	-0.0017	0.0041	-0.0036	-0.0004	-0.0070	-0.0047

Table 6: Detected discrepancies (I.E., three shifts and three rotations) between the reconstructed strip pairs using the estimated system parameters from the LMS calibration procedure based on flight lines from a single flying height

Using flight lines at 2000m flying height in the calibration						Using flight lines at 1000m flying height in the calibration					
11&12 (2000m)			13&14 (2000m)			5&6 (1000m)			5&7 (1000m)		
X_T' (m)	Y_T' (m)	Z_T' (m)	X_T' (m)	Y_T' (m)	Z_T' (m)	X_T' (m)	Y_T' (m)	Z_T' (m)	X_T' (m)	Y_T' (m)	Z_T' (m)
0.10	0.04	0.00	0.15	0.00	0.01	0.03	0.00	-0.01	0.02	-0.10	0.00
Ω' (°)	Φ' (°)	K' (°)	Ω' (°)	Φ' (°)	K' (°)	Ω' (°)	Φ' (°)	K' (°)	Ω' (°)	Φ' (°)	K' (°)
0.00	0.00	0.00	-0.0007	-0.0032	0.0091	-0.0011	0.0099	-0.0024	0.0002	0.0035	-0.0024

Table 7: Detected discrepancies (I.E., three shifts and three rotations) between the reconstructed strip pairs that are acquired from 2000m flying height using the estimated system parameters from the LMS calibration based on acquired flight lines from a 1000m flying height

11&12 (2000m)			13&14 (2000m)		
X_T' (m)	Y_T' (m)	Z_T' (m)	X_T' (m)	Y_T' (m)	Z_T' (m)
-0.42	0.42	0.00	-0.32	0.38	0.00
Ω' (°)	Φ' (°)	K' (°)	Ω' (°)	Φ' (°)	K' (°)
0.0005	0.0165	0.0003	-0.0005	0.0105	0.0028

Table 8: Remaining biases in the system parameters after the traditional and LMS calibration as determined by the diagnostic component of the quality control

Biases in the system parameters	δΔX(°)	δΔY(°)	δΔω(°)	δΔφ(°)	δΔκ(°)	δS
Traditional calibration	-0.07	-0.19	0.017	-0.002	0.054	-0.000050
LMS calibration (using flight lines flown at 1000 and 2000m flying height)	-0.06	-0.19	0.0098	0.003	0.003	-0.000046

Table 9: Detected discrepancies (i.e., THREE SHIFTS AND THREE ROTATIONS) between the reconstructed strip pairs after removing the impact of the estimated remaining biases in system parameters (from the traditional method) by the diagnostic component of the quality control procedure

11&12 (2000m)			13&14 (2000m)			5&6 (1000m)			5&7 (1000m)		
X_T' (m)	Y_T' (m)	Z_T' (m)	X_T' (m)	Y_T' (m)	Z_T' (m)	X_T' (m)	Y_T' (m)	Z_T' (m)	X_T' (m)	Y_T' (m)	Z_T' (m)
-0.08	0.02	0.00	-0.01	0.03	0.02	0.12	-0.02	-0.02	0.02	-0.10	0.00
Ω' (°)	Φ' (°)	K' (°)	Ω' (°)	Φ' (°)	K' (°)	Ω' (°)	Φ' (°)	K' (°)	Ω' (°)	Φ' (°)	K' (°)
0.0007	0.0031	-0.0003	0.0000	-0.0027	0.0044	-0.0006	-0.0073	-0.0018	0.0001	0.0035	0.0006

TABLE 10 – Detected discrepancies (I.E., three shifts and three rotations) between the reconstructed strip pairs using the estimated system parameters from the lms calibration after correcting the lever arm components in the along-flight and across-flight directions

11&12 (2000m)			13&14 (2000m)			5&6 (1000m)			5&7 (1000m)		
X_T' (m)	Y_T' (m)	Z_T' (m)	X_T' (m)	Y_T' (m)	Z_T' (m)	X_T' (m)	Y_T' (m)	Z_T' (m)	X_T' (m)	Y_T' (m)	Z_T' (m)
-0.10	0.02	-0.01	-0.02	0.01	0.01	0.09	-0.02	0.03	0.04	-0.10	0.03
Ω' (°)	Φ' (°)	K' (°)	Ω' (°)	Φ' (°)	K' (°)	Ω' (°)	Φ' (°)	K' (°)	Ω' (°)	Φ' (°)	K' (°)
0.0007	0.0038	-0.0006	-0.0003	0.0028	0.0088	-0.0009	-0.0009	-0.0023	0.0001	0.002	0.0003

- Traditional Calibration: Highly dependent on a calibration site with specific surveyed targets
- LMS Calibration: No control information required. Control information is only used for the range bias estimation, which needs to be performed occasionally using another piece of software.
- Flight configuration requirements:
- Traditional Calibration: Flight lines following specific scan angle configuration over a large building with known boundaries are used to estimate the angular offset (index error) and biases in the boresight pitch and roll angles. In addition, flight lines over an airport runway with surveyed ground control points are used to estimate the biases in the mirror angle scale and range.
- LMS Calibration: Project flight lines can be used. To maximize the accuracy of the estimated parameters, flight lines over an urban area are recommended (but are not mandatory). Also, flight lines in cross directions are recommended by the system manufacturer.

To evaluate/compare the performance of both calibration techniques, experimental results from a dataset acquired by an Optech ALTM 2050 system, with a configuration that satisfies the requirements of both calibration techniques as well as the diagnostic component of the quality control procedure, have been performed. Although the traditional calibration procedure can meet the system's accuracy specifications, the potential accuracy is not fully achieved. Significant improvement in the estimated system parameters could be observed when using the LMS calibration. To achieve the maximum accuracy, the lever arm should be accurately determined in the laboratory/platform calibrations since such parameters are not currently modeled in the LMS calibration. Moreover, using flight lines from different flying heights is recommended to reduce the impact of remaining biases in the lever arm component in the along-flight direction on the estimated boresight pitch angle.

The validity of the quality control procedure has been demonstrated by estimating the discrepancies among overlapping strip pairs and the remaining biases after applying the estimated parameters from the different calibration procedures. Therefore, the quality control procedure can also be thought of as a calibration technique, which can be performed by the end user without having access to the raw measurements and a manufacturer-provided software package. Future work will focus on demonstrating the improvements in the accuracy of the derived LiDAR point cloud when using more robust methodologies for the GPS/INS integration process as well as in a variety of terrain coverage and flight configuration scenarios.

Acknowledgements

Funding for the development of the quality control procedure was provided by a Discovery Grant from the Canadian Natural Science and Engineering Research Council (NSERC) and GEOIDE NCE. The authors would like also to thank CNPq (Conselho Nacional de Desenvolvimento Científico e Tecnológico) for the tax benefits provided by the law 8010/90, L.I. 12/1846474-1.

References

BURMAN, Helén. **Calibration and orientation of airborne image and laser scanner data using GPS and INS**. 2000. PhD Dissertation. KTH.

FILIN, S. **Calibration of spaceborne and airborne laser altimeters using natural surfaces**. 2001. PhD Dissertation, Department of Civil and Environmental Engineering and Geodetic Science, the Ohio-State University, Columbus, OH.

FRIESS, P. Toward a rigorous methodology for airborne laser mapping. **Proceedings EuroCOW,** 2006. p. 25-27.

HABIB, A.; BANG K.; KERSTING A. P.; LEE D. C. Error budget of LiDAR systems and quality

control of the derived data. **Photogrammetric Engineering and Remote Sensing,** v. 75, n. 9, p. 1093-1108, 2009.

HABIB, A.; KERSTING A. P.; BANG K.; LEE D. C. Alternative methodologies for the internal quality control of parallel LiDAR strips. **Geoscience and Remote Sensing, IEEE Transactions on**, v. 48, n. 1, p. 221-236, 2010a.

HABIB, A.; BANG K.; KERSTING A. P.; CHOW J. Alternative methodologies for LiDAR system calibration. **Remote Sensing**, v. 2, n. 3, p. 874-907, 2010b.

MORIN, Kristian Walker. **Calibration of airborne laser scanners**. 2002. M.S. thesis, Department of Geomatics Engineering, the University of Calgary, Calgary, Canada.

KERSTING, A. P. & MARTINS, M. **Relatório de Calibração Equipamento Laser Modelo ALTM 2050**. 2006. LACTEC – Instituto de Tecnologia para o Desenvolvimento, Curitiba, Paraná.

KERSTING, A. P. **Quality Assurance of Multi-Sensor Systems**. 2011. PhD Dissertation, Department of Geomatics Engineering, the University of Calgary, Calgary, Canada.

KERSTING, A. P.; HABIB, A.; BANG, K.; and SKALOUD, J. Automated approach for rigorous light detection and ranging system calibration without preprocessing and strict terrain coverage requirements. **Optical Engineering**, v. 51, n. 7, p. 076201-1-076201-19, 2012.

SCHENK, T. **Modeling and Analyzing Systematic Errors in Airborne Laser Scanners.** 2001. Technical Report in Photogrammetry No. 19, Ohio Sate University.

SKALOUD, J.; VALLET J.; KELLER K.; VEYSSIERE G.; KOELBL O. Rapid large scale mapping using handheld LiDAR/CCD/GPS/INS sensors on helicopters. In: **Proceedings of the 18th International Technical Meeting of the Satellite Division of The Institute of Navigation (ION GNSS 2005)**, 2001. p. 2461-2467.

SKALOUD, J. & LICHTI D. Rigorous Approach to Bore-Sight Self-Calibration in Airborne Laser Scanning. **ISPRS Journal of Photogrammetry and Remote Sensing**, v. 61, n. 1, p. 47-59, 2006.

TOTH, C.K. Calibrating airborne lidar systems, In: **Proceedings of ISPRS Commission II Symposium**, Xi'an, China. 2002. p. 475-480.

WEHR, A. & LOHR U. Airborne laser scanning—an introduction and overview. **ISPRS Journal of Photogrammetry and Remote Sensing**, v. 54, n. 2, p. 68-82, 1999.